Circular Clustering in Fuzzy Approximation Spaces for Color Normalization of Histological Images

Pradipta Maji and Suman Mahapatra

***Abstract*— One of the foremost and challenging tasks in hematoxylin and eosin stained histological image analysis is to reduce color variation present among images, which may significantly affect the performance of computer-aided histological image analysis. In this regard, the paper introduces a new rough-fuzzy circular clustering algorithm for stain color normalization. It judiciously integrates the merits of both fuzzy and rough sets. While the theory of rough sets deals with uncertainty, vagueness, and incompleteness in stain class definition, fuzzy set handles the overlapping nature of histochemical stains. The proposed circular clustering algorithm works on a weighted hue histogram, which considers both saturation and local neighborhood information of the given image. A new dissimilarity measure is introduced to deal with the circular nature of hue values. Some new quantitative measures are also proposed to evaluate the color constancy after normalization. The performance of the proposed method, along with a comparison with other state-of-the-art methods, is demonstrated on several publicly available standard data sets consisting of hematoxylin and eosin stained histological images.**

***Index Terms*— Histological image analysis, color normalization, circular clustering, rough sets.**

I. Introduction

IN HISTOLOGY, microscopic images of tissue sections are examined to study the manifestation of diseases under consideration. The most important property of histological images is the enormous density of data, more cellular details, compared to radiological, cytological and other imaging modalities, which makes computer-aided diagnosis more accurate than other modalities. To facilitate pathologists' examination, tissue samples are stained with multiple contrasting histochemical reagents, which in turn highlight different tissue structures and cellular features [1]. Hence, color in pathology plays a pivotal role as a good indicator of histological components. Computer-aided diagnosis can significantly eliminate imperfection associated with human interpretation in histological analysis of prostate, cervical and breast cancer diagnosis [2].

One of the most common and primary problems of histological tissue analysis is the inadmissible inter and intra-specimen variation in stained tissue color. There are a number of factors associated with the inconsistency in color representation, such as manual sectioning of the tissue samples during specimen preparation, orientation of the lens aperture, inconsistency in staining procedure, variation in quality of stains obtained from different manufacturers, storage condition, inter-patient and inter-biopsy staining variations and so on. Consequently, numerical features extracted from histological images may lead to difficulty in image interpretation by automated systems, trained on a specific stain color appearance [3], [4]. Although some methods have been proposed to maintain color consistency in images that follow Lambertian (reflective) model of image formation [5], these methods become irrelevant for histological images formed via transmitted light microscopy.

With the advancement of technology, some recent studies have ensured the importance of color features in quantitative analysis of histological images [6], [7]. One of the simplest approaches of color normalization is histogram specification [8]. Recently, variations of histogram specification have been proposed in [9] and [10] based on color map quantile matching and histogram landmark matching, respectively. Since histogram specification based approaches ignore both local neighborhood information and actual causes of color disagreement, significant amount of histological information is lost after color normalization. In [11], each image is transformed from correlated RGB to decorrelated L$\alpha\beta$ color space [12], and query image channels are standardized based on the template image channel statistics. In [13], the images are first converted from RGB to HSI color space, and based on the angular differences, the query image channels are normalized using template image channels. The approaches reported in [11], [13] assume that the proportions of tissue compartments are identical across the images being normalized, which is not a legitimate assumption in histological image analysis.

The stain separation based color normalization methods try to address the above problems to a great extent. Based on the relationship between stain amount and light absorption, as given by the Beer-Lambert law of colorimetry [14], the color deconvolution method is used in [15], [16] to extract

Manuscript received October 22, 2019; revised November 21, 2019; accepted November 26, 2019. Date of publication December 2, 2019; date of current version April 30, 2020. *(Corresponding author: Pradipta Maji.)*

The authors are with the Biomedical Imaging and Bioinformatics Lab, Machine Intelligence Unit, Indian Statistical Institute, Kolkata 700108, India (e-mail: pmaji@isical.ac.in; sumancse_r@isical.ac.in).

This article has supplementary downloadable material available at http://ieeexplore.ieee.org, provided by the authors.

Color versions of one or more of the figures in this article are available online at http://ieeexplore.ieee.org.

Digital Object Identifier 10.1109/TMI.2019.2956944

light absorbing stains. Accordingly, stain color appearance map and corresponding stain density map are estimated using the control slides. For estimating image-specific stain concentration map, global stain color descriptor and local pixel-level RGB information are used in [3] as feature map, while relevance vector machine is used as supervised color classifier. A major drawback of color deconvolution based normalization methods is their dependency on the availability of supervised control slides. Based on the color linear unmixing model of fluorescence imaging, which corresponds to the blind source separation problem, several approaches have been proposed [17], [18]. In the plane fitting (PF) approach [19], a geometric solution has been proposed to achieve stain decomposition using singular value decomposition followed by thresholding. The modified PF approach [20] uses prior knowledge on color vector direction for the estimation of accurate stain vectors. The major drawback of the PF based approaches is that the associated thresholds and control parameters are prefixed and cannot be updated adaptively according to image content, which may lead to faulty stain decomposition.

In a blind color decomposition method [21], input image is first transformed from RGB color space to Maxwellian chromaticity plane for the identification of reference colors from image information. However, the drawback of this approach is that it ignores the presence of weak stains in the image and is likely to be affected by achromatic portions while estimating the weak stain spectra. In [22], saturation-weighted (SW) hue histogram is computed from each image and k-means is employed to perform pixel clustering. In [23], circular thresholding [24] was applied on the SW hue histogram to extract cluster information, and respective stain matrix was estimated. Vahadane *et al.* [25] proposed a blind stain separation method based on sparse non-negative matrix factorization (NMF). As these methods ignore color mixing due to stain overlap and hardly assign each pixel to a particular stain cluster, the resultant stain decomposition is supposed to be less accurate. Recently, deep-learning approaches, particularly based on adversarial networks [26]–[29], have become popular for stain color normalization of histological images. Under this framework, a model is able to learn image-specific color transformation, data-specific staining properties and task-specific networks [27].

One of the main problems in histological image analysis is uncertainty. Some of the sources of this uncertainty include incompleteness and vagueness in stain class definition, as well as overlapping characteristics of histochemical stains. In [30], Li *et al.* proposed a circular mixture modeling based stain decomposition method, which considers physical constraints such as non-negativity of the factor matrices, and the overlapping nature of associated stains. It assumes that each stain class follows circular normal or von Mises distribution. This distribution attains highest probability density value only at its mean. So, a single hue value, which is equal to the mean, ensures the definite belongingness of a pixel to the stain class, as it can only possess highest probability of belongingness to the stain class. However, a single hue value can never represent a stain class perfectly. In reality, a specific range or a set of hue values around mean represents the definite belongingness of pixels to a stain class. The probability of belongingness for a pixel to the stain class will be highest if it attains any of the hue values within that range, and will decrease if it deviates further from the bound. Hence, instead of using only von Mises distribution to represent a stain class for histological images, each stain class should be defined using two sets: a core region, consisting of multiple hue values to represent definite belongingness of pixels, and an overlapping boundary region. In this background, rough sets [31] and fuzzy set [32], together may be effective to introduce the above concept while handling uncertainty present in histological image analysis. Since the integrated approach has the capability of providing a stronger paradigm for uncertainty handling, it has greater promise in image analysis, where fuzzy set and/or rough sets [33] are being effectively used and proved to be successful.

In this regard, the paper presents a new circular clustering algorithm, termed as rough-fuzzy circular clustering, for color normalization of histological images. The proposed algorithm assumes that each stain class is represented by a centroid, a crisp lower approximation, and a fuzzy boundary. While the membership function of fuzzy set enables efficient handling of overlapping stain classes, the concept of lower approximation and boundary region of rough sets deals with uncertainty, vagueness, and incompleteness in stain class definition. Integrating judiciously the merits of both saturation-weighted hue histogram and local neighborhood information of hue image, the proposed algorithm works on a weighted hue histogram in HSI color space. A new dissimilarity measure is introduced to deal with the circular nature of hue values. Some new quantitative measures are also proposed to evaluate the color constancy after normalization. The efficacy of the proposed algorithm, along with a comparison with existing algorithms, is demonstrated on benchmark histological image sets.

II. Proposed Stain Color Normalization Method

Stain decomposition is a process that estimates the stain color appearance map and density proportions at each pixel (stain density map) in a histological image. In the proposed method, the stain decomposition problem is formulated following transmission light microscopy [22] based image model. Geometrically, as the stain vectors intersect at the origin in the optical density (OD) space, an image is first converted to OD domain and then factorized to obtain the stain color appearance map and corresponding stain density map. Fig. 1 depicts different components of the proposed method. To estimate the stain color appearance map, a rough-fuzzy circular clustering algorithm is proposed in fuzzy approximation spaces. It is based on a new dissimilarity measure that follows next.

A. Circular Dissimilarity Measure

The color distribution of the image pixels in hue channel of the HSI color space is studied to achieve robustness. It is based on the intuition that hue is a natural descriptor of the color distribution in a color image. As in HSI space, chroma information (hue and saturation) is separated from the luma information (illumination), color analysis in the hue domain is invariant to irregular illumination. So, each histological image is first converted from RGB to HSI color space for

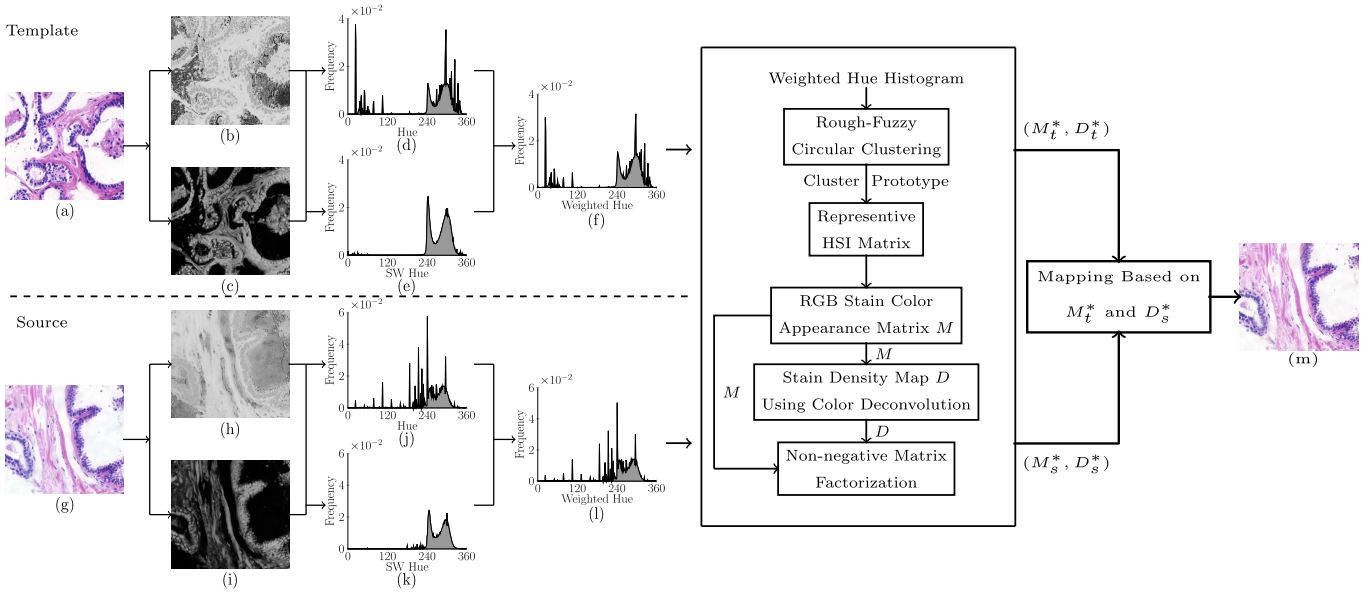

Fig. 1. Proposed method for stain color normalization of histological images: (a) and (g) represent the template and source images, respectively. (b) and (h) depict the corresponding hue information, while (c) and (i) are the respective saturation images. The hue histograms of template and source images are given in (d) and (j), while saturation-weighted (SW) hue histograms are depicted in (e) and (k), respectively. (f) and (l) are the weighted hue histograms of template and source images, respectively, obtained from corresponding hue and SW hue histograms. The proposed rough-fuzzy circular clustering algorithm accepts weighted hue histograms of (f) and (l) as inputs and generates cluster prototypes as corresponding outputs. The cluster prototypes of both template and source images are used to generate corresponding HSI matrices. The stain color appearance matrix M and stain density map D are estimated from HSI matrix, where non-negative matrix factorization ensures non-negativity constraint of both M and D. Based on M and D, the color normalized source image, corresponding to (g), is produced and reported in (m).

further analysis. In this section, a new dissimilarity measure is introduced to deal with the circular nature of hue values.

Let θ_i and θ_j denote the i-th and j-th hue values, respectively, and $\theta_0 = (\theta_i - \theta_j)$ represents the difference between these two hue values. In general, the similarity or dissimilarity between θ_i and θ_j can be computed by either $\cos(\theta_0)$ or $(1 - \cos(\theta_0))$. However, the cosine function fails to model concentration of values near its peak. The area under the curve of cosine function can be varied, without affecting its periodicity, by multiplying a parameter κ with $\cos(\theta_0)$. Based on the above concept, a new dissimilarity measure, denoted by $d(\theta_i, \theta_j)$, is defined as follows:

$$d(\theta_i, \theta_j) = \log\left(\int_0^{2\pi} \exp(\kappa \cos\theta) d\theta\right) - \kappa \cos(\theta_i - \theta_j);$$
$$\Rightarrow d(\theta_i, \theta_j) = \log(2\pi I_0(\kappa)) - \kappa \cos(\theta_i - \theta_j); \quad (1)$$

where $I_0(.)$ is the modified Bessel function of first kind and order zero, defined as:

$$I_0(\kappa) = \frac{1}{2\pi} \int_0^{2\pi} \exp(\kappa \cos\theta) d\theta. \quad (2)$$

From (1), the following properties can be derived for the proposed dissimilarity measure:

1) $d(\theta_i, \theta_j) = d(\theta_j, \theta_i)$;
2) $d(\theta_i, \theta_i) < d(\theta_i, \theta_j), \forall j \neq i$;
3) $d(\theta_i, \theta_k) \leq d(\theta_i, \theta_j) + d(\theta_j, \theta_k), \forall \theta_i, \theta_j, \theta_k \in [0, 2\pi)$.

The first two properties are trivial. The first one ensures the symmetric property of the proposed dissimilarity measure. The second one states that whenever θ_i and θ_j coincide, the dissimilarity measure is the minimum. The third axiom, the triangle inequality, seems to be intuitively evident, but this property is a hard one to satisfy.

B. Weighted Hue Histogram

The proposed rough-fuzzy circular clustering algorithm considers a weighted hue histogram H, instead of standard hue histogram, to estimate the stain class representatives. The weighted hue histogram H judiciously integrates the merits of both saturation-weighted hue histogram H^{sw} and local neighborhood information. In [34], it has been shown that the standard hue histogram consists of a number of sharp ridges attributed by achromatic pixels. So, the hue values, corresponding to achromatic region, are ill-defined and insignificant for the pixels that contain small saturation values. As a result, analysis of color distribution on a standard hue histogram, corrupted by these insignificant pixels, yields insignificant and faulty output. So, the effects of these achromatic pixels on the standard hue histogram can be reduced by computing saturation-weighted hue histogram H^{sw} [34], as follows:

$$H^{sw}(\theta) = \sum_{k \in \mathcal{I}} s_k \delta(\theta, h_k); \quad (3)$$

$$\text{where} \quad \delta(\theta, h_k) = \begin{cases} 1 & \text{if } \theta = h_k \\ 0 & \text{otherwise.} \end{cases} \quad (4)$$

Here, $\mathcal{I}$ represents a pathology image, s_k and h_k denote, respectively, saturation and hue value corresponding to the k-th pixel in the HSI color space. In order to consider the local neighborhood information of a pixel in standard hue image h, the proposed algorithm introduces a α-controlled hue image,

following the model of Szilagyi *et al.* [35]. The proposed α-controlled mean filtered hue image ξ can be obtained from the original hue image h as follows:

$$\xi_k = \frac{1}{1+\alpha}\left(h_k + \frac{\alpha}{|N_k|}\sum_{h_j \in N_k} h_j\right); \tag{5}$$

where ξ_k denotes the k-th pixel of the α-controlled hue image ξ and N_k represents the set of neighbors within a window around h_k. The parameter α controls the influence of the neighborhood information. A α-controlled approximated histogram H^α can be computed from the α-controlled hue image ξ, where $H^\alpha(\theta)$ denotes the number of pixels in ξ having hue value θ. Combining both saturation-weighted hue histogram H^{sw} and α-controlled approximated histogram H^α, a weighted hue histogram H is defined as follows:

$$H(\theta) = \frac{1}{2}\left[H^{sw}(\theta) + H^\alpha(\theta)\right]. \tag{6}$$

C. Rough-Fuzzy Circular Clustering

The proposed rough-fuzzy circular clustering algorithm assumes that each stain class is represented by a centroid, a crisp lower approximation, and a fuzzy boundary. Let $\underline{A}(\beta_i)$ and $B(\beta_i)$ denote the lower approximation and boundary region of the i-th stain class β_i. The upper approximation $\overline{A}(\beta_i)$ of stain class β_i is given by $\overline{A}(\beta_i) = [\underline{A}(\beta_i) \cup B(\beta_i)]$. According to the definitions of lower approximation and boundary region of rough sets [31], if the j-th hue value θ_j belongs to the lower approximation $\underline{A}(\beta_i)$ of the i-th stain class β_i, then θ_j does not belong to lower approximations and boundary regions of any other stain classes. That is, θ_j definitely belongs to the stain class β_i. Hence, the weights of hue values lying in lower approximation of a stain class should be independent of other centroids and stain classes, and should not be coupled with their similarity with respect to other centroids. On the other hand, if a hue value θ_j belongs to the boundary region $B(\beta_i)$ of the i-th stain class β_i, then θ_j possibly belongs to β_i and potentially belongs to another stain class.

The proposed rough-fuzzy circular clustering algorithm with parameter set ψ divides the weighted hue histogram H, corresponding to a histology image $\mathcal{I}$, into c stain classes by minimizing the following objective function:

$$J_{\mathrm{RF}}(\psi) = \sum_{i=1}^{c}\left[\omega \times J_i^L(\psi) + (1-\omega)\times J_i^B(\psi)\right]; \tag{7}$$

where ω regulates the relative importance between lower approximation and boundary region of each stain class, and

$$J_i^L(\psi) = \sum_{\theta_j \in \underline{A}(\beta_i)} [\log(2\pi I_0(\kappa_i)) - \kappa_i \cos(\theta_j - \mu_i)]H(\theta_j);$$

$$J_i^B(\psi) = \sum_{\theta_j \in B(\beta_i)} v_{ij}^m [\log(2\pi I_0(\kappa_i)) - \kappa_i \cos(\theta_j - \mu_i)]H(\theta_j) + \sum_{\theta_j \in B(\beta_i)} [v_{ij}^m \log(v_{ij}^m) - v_{ij}^m]H(\theta_j).$$

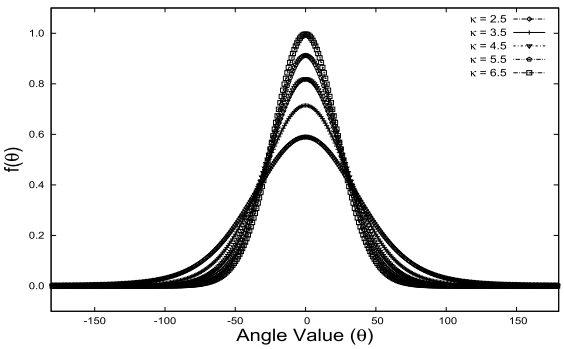

Fig. 2. von Mises distribution for different values of parameter κ.

Here θ_j and μ_i represent the j-th hue and centroid of the i-th stain class β_i, v_{ij} denotes fuzzy membership of the j-th hue into i-th class β_i, $m \in [1, \infty)$ is the fuzzifier, κ_i is the concentration parameter corresponding to β_i, and $I_0(\cdot)$ is the modified Bessel function of first kind and order zero, defined in (2). So, the parameter set ψ is given as $\psi = \{\mu_i, \kappa_i, v_{ij}\}$. Note that the term $[v_{ij}^m \log(v_{ij}^m) - v_{ij}^m]$ is a monotonically decreasing function of v_{ij} in $[0, 1]$, and forces v_{ij} to be as large as possible to avoid the trivial solution.

1) Estimation of Membership Function: To estimate the fuzzy membership v_{ij} of the j-th hue into i-th stain class β_i, (7) is partially differentiated with respect to v_{ij} as follows:

$$\begin{aligned}
&\frac{\partial J_{\mathrm{RF}}(\psi)}{\partial v_{ij}} = 0;\\
\Rightarrow\ & m v_{ij}^{m-1}[\log(2\pi I_0(\kappa_i)) - \kappa_i \cos(\theta_j - \mu_i)]H(\theta_j)\\
&+ m v_{ij}^{m-1}\log(v_{ij}^m)H(\theta_j) = 0;\\
\Rightarrow\ & \log(v_{ij}^m) = \kappa_i \cos(\theta_j - \mu_i) - \log(2\pi I_0(\kappa_i));\\
\Rightarrow\ & \log(v_{ij}^m) = \log\left[\frac{\exp\{\kappa_i \cos(\theta_j - \mu_i)\}}{2\pi I_0(\kappa_i)}\right];\\
\Rightarrow\ & v_{ij} = \left[\frac{\exp\{\kappa_i \cos(\theta_j - \mu_i)\}}{2\pi I_0(\kappa_i)}\right]^{\frac{1}{m}}.
\end{aligned} \tag{8}$$

From (8), it is evident that the fuzzy membership function follows von Mises distribution, which is a variant of the Gaussian distribution in circular domain and is defined next.

Definition 1: A circular random variable θ is said to follow von Mises or circular normal distribution, if it has the probability density function defined as follows [36]:

$$vM(\mu, \kappa) = \frac{1}{2\pi I_0(\kappa)}\exp\{\kappa \cos(\theta - \mu)\}; \tag{9}$$

where $\mu \in [0, 2\pi)$ and $\kappa > 0$ denote the mean direction and concentration parameter, respectively. Fig. 2 presents the von Mises distribution for different values of concentration parameter κ.

2) Computation of Cluster Prototype: The new centroid is computed based on the weighted average of the crisp lower approximation and fuzzy boundary region of each stain class. The centroid, corresponding to each stain class β_i, is computed

by solving (7) with respect to μ_i, as follows:

$$\frac{\partial J_{\mathrm{RF}}(\psi)}{\partial \mu_i} = 0; \Rightarrow \omega \times \sum_{\theta_j \in \underline{A}(\beta_i)} \sin(\theta_j - \mu_i) H(\theta_j) + (1-\omega) \times \sum_{\theta_j \in B(\beta_i)} \nu_{ij}^m \sin(\theta_j - \mu_i) H(\theta_j) = 0;$$

$$\Rightarrow \mu_i = \arctan\left[\frac{\omega \times \mathcal{A}_1 + (1-\omega) \times \mathcal{A}_2}{\omega \times \mathcal{B}_1 + (1-\omega) \times \mathcal{B}_2}\right];$$

$$\text{where } \mathcal{A}_1 = \sum_{\theta_j \in \underline{A}(\beta_i)} \sin(\theta_j) H(\theta_j);$$

$$\mathcal{A}_2 = \sum_{\theta_j \in B(\beta_i)} \nu_{ij}^m \sin(\theta_j) H(\theta_j);$$

$$\mathcal{B}_1 = \sum_{\theta_j \in \underline{A}(\beta_i)} \cos(\theta_j) H(\theta_j);$$

$$\text{and } \mathcal{B}_2 = \sum_{\theta_j \in B(\beta_i)} \nu_{ij}^m \cos(\theta_j) H(\theta_j). \quad (10)$$

From (10), it is observed that the computation of centroid is dependent on the choice of the parameter ω. Since the hue values lying in lower approximation region definitely belong to a certain stain class, they are supposed to be assigned a higher weightage ω compared to $(1-\omega)$ corresponding to the hues lying in boundary region.

3) Estimation of Concentration Parameter: To estimate the concentration parameter κ_i, corresponding to the i-th stain class β_i, (7) is partially differentiated with respect to κ_i, as follows:

$$\frac{\partial J_{\mathrm{RF}}(\psi)}{\partial \kappa_i} = 0;$$

$$\Rightarrow \omega \times \sum_{\theta_j \in \underline{A}(\beta_i)} \left\{\frac{I_0'(\kappa_i)}{I_0(\kappa_i)} - \cos(\theta_j - \mu_i)\right\} H(\theta_j) + (1-\omega) \times \sum_{\theta_j \in B(\beta_i)} \nu_{ij}^m \left\{\frac{I_0'(\kappa_i)}{I_0(\kappa_i)} - \cos(\theta_j - \mu_i)\right\} H(\theta_j) = 0;$$

$$\Rightarrow \frac{I_1(\kappa_i)}{I_0(\kappa_i)} \left\{\omega \times \sum_{\theta_j \in \underline{A}(\beta_i)} H(\theta_j) + (1-\omega) \times \sum_{\theta_j \in B(\beta_i)} \nu_{ij}^m H(\theta_j)\right\} = \left\{\omega \times \sum_{\theta_j \in \underline{A}(\beta_i)} \cos(\theta_j - \mu_i) H(\theta_j) + (1-\omega) \times \sum_{\theta_j \in B(\beta_i)} \nu_{ij}^m \cos(\theta_j - \mu_i) H(\theta_j)\right\}$$

as $I_0'(\kappa_i) = \frac{d}{d\kappa_i}(I_0(\kappa_i)) = I_1(\kappa_i)$. Let $\mathsf{T}(\kappa_i) = \frac{I_1(\kappa_i)}{I_0(\kappa_i)}$. So,

$$\kappa_i = \mathsf{T}^{-1}\left[\frac{\omega \times \mathcal{X}_1 + (1-\omega) \times \mathcal{X}_2}{\omega \times \mathcal{Y}_1 + (1-\omega) \times \mathcal{Y}_2}\right];$$

$$\text{where } \mathcal{X}_1 = \sum_{\theta_j \in \underline{A}(\beta_i)} \cos(\theta_j - \mu_i) H(\theta_j);$$

$$\mathcal{X}_2 = \sum_{\theta_j \in B(\beta_i)} \nu_{ij}^m \cos(\theta_j - \mu_i) H(\theta_j);$$

$$\mathcal{Y}_1 = \sum_{\theta_j \in \underline{A}(\beta_i)} H(\theta_j); \quad \text{and } \mathcal{Y}_2 = \sum_{\theta_j \in B(\beta_i)} \nu_{ij}^m H(\theta_j). \quad (11)$$

Here, $\mathsf{T}^{-1}(.)$ is approximated using numerical methods [36].

Each stain class β_i is characterized by the parameter set $\psi = \{\mu_i, \kappa_i, \nu_{ij}\}$. The cluster prototype μ_i is considered as the representative hue for the i-th stain class β_i. The parameter κ_i controls the concentration of hue values around the centroid μ_i of the stain class β_i. The fuzzy membership ν_{ij} of the j-th hue into i-th stain class β_i depends on both μ_i and κ_i.

D. Proposed Algorithm and Stain Color Normalization

Approximate optimization of $J_{\mathrm{RF}}(\psi)$ in (7) by the proposed rough-fuzzy circular clustering algorithm is performed based on Picard iteration through (8), (10) and (11). The process starts by initializing $\mu_i^{(0)}$, $\kappa_i^{(0)}$, and $\nu_{ij}^{(0)}$ for $(c-1)$ stain regions and one achromatic region. As hue is circular in nature, the circular thresholding method [24] is used to generate approximate partitions corresponding to achromatic region and different stain regions. The initial cluster prototype $\mu_i^{(0)}$ and concentration parameter $\kappa_i^{(0)}$, corresponding to both achromatic and stain regions, are computed from the weighted hue histogram H, based on the initial parameter estimation procedure reported in [30]. The fuzzy memberships of all hues are then calculated using (8). After computing ν_{ij} for c stain classes (including achromatic region) and n hue values, the values of ν_{ij} for each hue θ_j are sorted and the difference of two highest memberships of θ_j is compared with a threshold value λ. Let ν_{ij} and ν_{kj} be the highest and second highest memberships of θ_j. If $(\nu_{ij} - \nu_{kj}) > \lambda$, then $\theta_j \in \underline{A}(\beta_i)$, otherwise $\theta_j \in B(\beta_i)$ and $\theta_j \in B(\beta_k)$. After assigning all hues in lower approximations or boundary regions of different stain classes based on λ, memberships ν_{ij} of the hues are modified. The values of ν_{ij} are set to 1 for the hues belonging to lower approximations, while those in boundary regions remain unchanged. The new centroids of the stain classes are calculated as per (10), while corresponding concentration parameters are computed using (11). The main steps of proposed rough-fuzzy circular clustering algorithm are as follows:

1) Initialize $\mu_i^{(0)}$ and $\kappa_i^{(0)}$ $(1 \le i \le c-1)$ for $(c-1)$ stain regions and $\mu_{ac}^{(0)}$ and $\kappa_{ac}^{(0)}$ for achromatic region.
2) Choose values for fuzzifier m, threshold λ and tolerance value ϵ. Set iteration counter $t = 1$.
3) Compute ν_{ij} for c stain classes and n hues using (8).
4) If ν_{ij} and ν_{kj} be the two highest memberships of θ_j and $(\nu_{ij} - \nu_{kj}) > \lambda$, then $\theta_j \in \underline{A}(\beta_i)$; otherwise $\theta_j \in B(\beta_i)$ and $\theta_j \in B(\beta_k)$.
5) Modify ν_{ij} considering lower approximation and boundary regions for c stain classes and n hues.
6) Compute new centroid μ_i as per (10).
7) Compute concentration parameter κ_i using (11).
8) Repeat steps 3 to 7 until $|\nu_{ij}^{(t)} - \nu_{ij}^{(t-1)}| < \epsilon$.

The proposed circular clustering algorithm partitions the hue values into two regions, namely, lower approximation and boundary region, based on the value of λ. In practice, the following definition of λ works well:

$$\lambda = \frac{1}{n}\sum_{j=1}^{n}(\nu_{ij}^{(0)} - \nu_{kj}^{(0)}); \quad (12)$$

where n is the total number of hues, $v_{ij}^{(0)}$ and $v_{kj}^{(0)}$ are the highest and second highest memberships of θ_j at $t = 0$. So, λ represents the average difference of two highest memberships of all hue values present in an image. A good clustering procedure should make the value of λ as high as possible.

The stain color appearance map can be computed from the centroid of each stain class. The cluster prototype μ_i, $i = 1, 2, \cdots, c$, estimated by the proposed rough-fuzzy circular clustering, is considered as the representative hue h_i for the i-th stain class β_i. The saturation-weighted statistics, described in [22], is used to compute the corresponding saturation s_i and intensity v_i for obtaining the stain representative color. The representative color $I_i^{\text{hsi}} = [h_i, s_i, v_i]^T$, corresponding to the i-th stain class, in HSI domain is first converted to RGB color space: $I_i^{\text{rgb}} = F_{\text{hsi}}^{\text{rgb}}(I_i^{\text{hsi}})$, where $F_{\text{hsi}}^{\text{rgb}}(.)$ denotes a function for converting a stain vector from HSI domain to RGB domain. The absorption vector corresponding to I_i^{rgb} in OD domain is given as $M_i^{\text{rgb}} = \log(I^b/I_i^{\text{rgb}})$, where I^b represents the intensity value corresponding to a background pixel. The stain density value, associated with pixel p, can be computed using the following relation:

$$D^{\text{rgb}}(p) = (M^{\text{rgb}})^{-1}[\log(I^b/I(p))]. \tag{13}$$

However, in OD domain, the image colors are represented as the non-negative combination of c stain vectors associated with the staining routine. Due to the non-negativity constraint of both stain color appearance matrix M and stain density map D, NMF is utilized to refine candidate stain decomposition solution by minimizing the following decomposition error:

$$\{\acute{M}, \acute{D}\} = \arg \min_{M \succeq 0, D \succeq 0} || \log(I^b/I) - MD ||^2; \tag{14}$$

where $\succeq 0$ denotes element-wise non-negativity of the matrix.

E. Convergence Analysis

In this section, a mathematical analysis on the convergence condition of the proposed rough-fuzzy circular clustering algorithm is presented. To examine the convergence property of the proposed algorithm, the Hessian (second order partial derivative) matrices with respect to the parameters involved in the objective function are computed and then checked whether the Hessian matrices are positive definite or not. The second order partial derivative of the objective function in (7) with respect to the cluster centroid μ_i leads to

$$\frac{\partial^2 J_{\text{RF}}(\psi)}{\partial \mu_i^2} = \omega \times U_i + (1 - \omega) \times V_i; \tag{15}$$

$$\text{where} \quad U_i = \sum_{\theta_j \in \underline{A}(\beta_i)} \kappa_i \cos(\theta_j - \mu_i) H(\theta_j); \tag{16}$$

$$\text{and} \quad V_i = \sum_{\theta_j \in B(\beta_i)} \kappa_i v_{ij}^m \cos(\theta_j - \mu_i) H(\theta_j). \tag{17}$$

It is evident that $\kappa_i > 0 \ \forall i$, $v_{ij}^m \geq 0$, $\cos(\theta_j - \mu_i) \geq 0$ and $H(\theta_j) \geq 0 \ \forall \theta_j$. Hence, for each cluster β_i, $U_i > 0$ and $V_i > 0$. Also, it can be easily verified that, $\forall k \neq i$,

$$\frac{\partial^2 J_{\text{RF}}(\psi)}{\partial \mu_k \partial \mu_i} = 0. \tag{18}$$

Hence, it is clear from (18) that all the off-diagonal entries in the respective Hessian matrices are 0. The proposed algorithm is guaranteed to converge if the Hessian matrix with respect to μ_i is diagonally dominant [37]. This is a sufficient condition, not a necessary one. If the Hessian matrix is not diagonally dominant, the iteration may or may not converge. The Hessian matrix corresponding to (16) is given by $\mathcal{P} = \text{diag}\{U_1, \cdots, U_i, \cdots, U_c\}$ and the matrix corresponding to (17) is given by $\mathcal{Q} = \text{diag}\{V_1, \cdots, V_i, \cdots, V_c\}$.

It can be easily observed that the Hessian matrices $\mathcal{P}$ and $\mathcal{Q}$ are diagonally dominant. So, $\mathcal{P}$ and $\mathcal{Q}$ are certainly positive definite matrices. Hence, all the eigenvalues corresponding to $\mathcal{P}$ and $\mathcal{Q}$ are positive. Under this condition, the iterative algorithm would converge to at least a local optimum solution if (10) was repetitively applied keeping both v_{ij} and κ_i constant. Similarly, it can be easily shown that the Hessian matrices with respect to both v_{ij} and κ_i are diagonal positive definite matrices. Intuitively, the objective function $J_{\text{RF}}(\psi)$ reduces in all steps corresponding to (8), (10) and (11), which makes the system strictly descent. It ensures the convergence of the proposed rough-fuzzy circular clustering algorithm.

III. Quantitative Measures

One of the important criteria of color normalization is to reduce the within-image as well as between-image color variation of a single biopsy set for a particular region of interest (ROI). It is assumed that the tissue specimens within the same biopsy set have undergone same staining treatment and thus they must exhibit similar color distribution. Though, normalized median intensity (NMI) [38] evaluates the color consistency of a specific ROI within an image, it does not capture the color consistency of the ROI among images within the same biopsy set. In order to address the above problem, two new quantitative indices are introduced next to evaluate the performance of different color normalization methods.

A. Between-Image Color Constancy Index

The between-image color constancy (BiCC) index of an image I, belonging to a biopsy set S, is defined as follows:

$$\text{BiCC}(I) = \frac{1}{2(|S| - 1)} \times \sum_{J \neq I} \left\{ \frac{\underset{i \in \text{ROI}(I)}{\text{median}}\{W(i)\} + \underset{j \in \text{ROI}(J)}{\text{median}}\{W(j)\}}{\max\left\{ \underset{i \in \text{ROI}(I)}{\max}\{W(i)\}, \underset{j \in \text{ROI}(J)}{\max}\{W(j)\} \right\}} \right\}; \tag{19}$$

where $W(i)$ denotes the average of (R, G, B) intensities for the i-th pixel corresponding to the ROI of image I. If the between-image color constancy is maintained after color normalization, it is expected that the median and maximum average intensity values, corresponding to ROIs of images I and J, would exhibit a close proximity. So, a good color normalization algorithm should make the value of BiCC as high as possible. The value of BiCC lies in between 0 and 1.

B. Within-Set Color Constancy Index

The within-set color constancy (WsCC) index for a biopsy set S is defined as follows:

$$\mathrm{WsCC}(S) = \frac{1}{|S|}\sum_{I\in S}\mathrm{NMI}(I) \times \mathrm{BiCC}(I); \tag{20}$$

where $\mathrm{NMI}(I)$ is the normalized median intensity of image I and $\mathrm{BiCC}(I)$ is the between-image color constancy of image I with respect to the biopsy set S. NMI is defined as follows:

$$\mathrm{NMI}(I) = \frac{\underset{i\in \mathrm{ROI}(I)}{\mathrm{median}}\{W(i)\}}{\underset{i\in \mathrm{ROI}(I)}{\max}\{W(i)\}}. \tag{21}$$

So, if the color constancy is maintained after normalization, then it is expected that the median and maximum of the average intensity values, corresponding to a particular ROI of image I, would be close enough; which indicates a high value of NMI. Also, the value of NMI ranges from 0 to 1. So, a good color normalization algorithm should make the WsCC for a biopsy set S high as both NMI and BiCC of a particular image, belonging to the biopsy set S, eventually possess high values. The value of WsCC varies in between 0 and 1.

IV. Performance Analysis

The performance of the proposed rough-fuzzy circular clustering based stain separation and color normalization method is studied extensively and compared with that of

- several state-of-the-art stain separation methods, namely, plane fitting (PF) [19], enhanced plane fitting (EPF) [39], structure-preserving color normalization (SPCN) [25], expectation-maximization (EM) algorithm [30], and the method named HTN due to Li and Plataniotis [22]; and
- different color normalization algorithms such as color transfer technique (ColTrans) [11], stain color description (SCD) [3], stain normalization using generative adversarial networks (SN-GAN) [26], StainGAN [29], and adversarial stain transfer (AST) [27], as well as PF [19], EPF [39], HTN [22], and SPCN [25].

To find out the optimum values of weight parameter ω and control parameter α for the proposed method, the value of ω is varied from 0.51 to 0.99, while that of α is varied in the range of 0.1 to 1.0, with an increment of 0.1. The optimum values of ω and α, for a particular image, are obtained using Silhouette index [40], as discussed in supplementary material.

To evaluate the performance of different stain separation and color normalization methods, following two publicly available histology image sets are used in the current study.

- UCSB Breast Cancer Cell Data: This data set, published by University of California, Santa Barbara [41], comprises of 32 non-cancerous benign cell and 26 cancerous malignant cell images, acquired from ten hematoxylin and eosin (H&E) stained breast cancer biopsy sets. Each image has a resolution of 896 × 768, and associated ground-truth with nuclei considered as ROIs. Since original images were stored in 24-bit nonlinear RGB format, all images are first converted to linear RGB domain [42].
- CMU Data: This data set, published by the bimagicLab in Carnegie Mellon University [39], contains three H&E stained 48-bit linear RGB format images with a resolution of 1280×1024. In addition, this data set consists of stain decomposition ground-truth, that is, separate H-stained and E-stained images corresponding to each image.

To evaluate the performance of different stain estimation and separation methods, standard deviation, symmetric Kullback-Leibler (KL) divergence and signal-to-noise ratio (SNR) are used, while normalized median intensity (NMI), between-image color constancy (BiCC) and within-set color constancy (WsCC) indices are used to evaluate color consistency of the specific ROI within a single biopsy set after color normalization. A brief description of experimental setup, definitions of quantitative indices used, and some important results are described in detail in the supplementary material.

A. Evaluation of Stain Vector Estimation

As the images within the same biopsy set undergo same type of staining routine and similar storage condition, a good spectral estimation algorithm should produce consistent stain vectors for the images of same biopsy set. The proposed circular clustering algorithm judiciously integrates the theory of rough sets, and merits of new circular dissimilarity measure and weighted hue histogram. To establish the importance of new dissimilarity measure over conventional cosine distance for stain vector estimation, extensive experiments are carried out on UCSB data set, and corresponding results are reported in Table I(a). In Table I(a), standard deviations (σ) of the estimated stain vectors, corresponding to ten biopsy sets, are summarized, where σ_{H} and σ_{E} represent the standard deviations of the estimated stain vectors of hematoxylin (H) stain and eosin (E) stain, respectively, computed over all images of the same biopsy set. The lower σ value of the respective RGB matrix element ensures the generation of consistent stain vectors for all images of a given biopsy set. The results reported in Table I(a) confirm that the proposed dissimilarity measure achieves lowest σ values in 19 and 27 cases, out of 30 cases each, for H-stain and E-stain, respectively.

In order to establish the significance of rough-fuzzy clustering over its hard ($\lambda = 0$) and fuzzy ($\lambda = 1$) counter parts, extensive experimentation is carried out on UCSB data set and corresponding results are reported in Table I(b). From the results reported in Table I(b), it can be easily observed that the proposed rough-fuzzy clustering algorithm attains lowest values of standard deviation in 18 and 25 cases for H-stain and E-stain, respectively, while hard and fuzzy clustering achieve lowest σ values in 3 and 0, and 9 and 6 cases, respectively. Finally, the performance of the proposed approach, in stain vector estimation, is extensively compared with that of several state-of-the-art stain separation methods, namely, PF [19], EPF [39], SPCN [25], EM [30] and HTN [22], and corresponding results are reported in Table II. From the results reported in Table II, it is seen that the proposed method attains lowest σ values in 14 and 13 cases, out of 30 cases each, for H-stain and E-stain, respectively. However, the PF, EPF, HTN, SPCN, and EM, respectively, provide lowest values of σ in only 0, 2, 7, 3, and 5 cases for H-stain and 4, 9, 1, 1, and 2 cases

TABLE I

PERFORMANCE ANALYSIS OF PROPOSED DISSIMILARITY MEASURE AND ROUGH-FUZZY CIRCULAR CLUSTERING ALGORITHM ON UCSB DATA SET: σ_X REPRESENTS THE STANDARD DEVIATION OF THE ESTIMATED STAIN VECTORS OF X-STAIN, COMPUTED OVER ALL IMAGES OF THE SAME BIOPSY SET, AND X $\in$ {H, E}. EACH VALUE IS REPRESENTED IN 10^{-2} SCALE. THE SMALLEST VALUE OF THE RESPECTIVE MATRIX ELEMENT IS MARKED IN BOLD

(a) Proposed Dissimilarity Measure and Cosine Distance

Different Biopsy Sets	Different Channels	Cosine Distance σ_H	Cosine Distance σ_E	Proposed Dissimilarity σ_H	Proposed Dissimilarity σ_E
ytma10_010704	Red	3.19	3.03	**2.84**	**2.35**
	Green	1.69	1.07	**1.27**	**0.89**
	Blue	**1.35**	2.30	1.64	**1.86**
ytma12_010804	Red	**3.38**	5.69	3.59	**4.14**
	Green	2.71	2.06	**2.67**	**1.60**
	Blue	**0.96**	1.10	**0.96**	**1.06**
ytma23_022103	Red	1.57	5.36	**1.37**	**4.00**
	Green	1.30	1.79	**1.07**	**1.51**
	Blue	0.67	1.36	**0.58**	**0.77**
ytma49_042003	Red	3.31	**2.53**	**2.66**	2.94
	Green	2.05	**0.55**	**1.72**	0.61
	Blue	0.98	1.07	**0.55**	**0.83**
ytma49_042203	Red	**2.64**	3.28	2.80	**2.77**
	Green	**2.07**	0.91	2.24	**0.58**
	Blue	**0.31**	**1.95**	0.54	2.06
ytma49_042403	Red	**1.78**	3.79	2.22	**2.30**
	Green	**1.07**	1.07	1.16	**0.93**
	Blue	0.66	0.88	**0.49**	**0.87**
ytma49_072303	Red	1.86	3.40	**1.04**	**1.73**
	Green	1.53	1.20	**0.73**	**0.76**
	Blue	0.30	0.83	**0.20**	**0.40**
ytma49_111003	Red	**2.34**	4.65	2.74	**3.60**
	Green	**2.07**	2.19	2.61	**1.58**
	Blue	0.99	1.85	**0.77**	**1.20**
ytma49_111303	Red	1.83	5.85	**1.38**	**3.35**
	Green	1.66	2.47	**1.31**	**1.69**
	Blue	0.92	1.72	**0.59**	**1.17**
ytma55_030603	Red	**2.65**	4.03	2.99	**3.60**
	Green	**2.29**	1.65	2.78	**1.46**
	Blue	1.16	1.76	**0.85**	**1.63**

(b) Hard, Fuzzy and Rough-Fuzzy Circular Clustering

Different Biopsy Sets	Different Channels	Hard σ_H	Hard σ_E	Fuzzy σ_H	Fuzzy σ_E	Rough-Fuzzy σ_H	Rough-Fuzzy σ_E
ytma10_010704	Red	13.44	4.68	4.05	2.72	**2.84**	**2.35**
	Green	5.54	8.69	2.00	1.03	**1.27**	**0.89**
	Blue	17.29	15.85	**1.47**	1.87	1.64	**1.86**
ytma12_010804	Red	13.24	5.93	**3.45**	4.26	3.59	**4.14**
	Green	5.67	10.92	2.75	1.90	**2.67**	**1.60**
	Blue	21.17	18.49	**0.87**	**0.97**	0.96	1.06
ytma23_022103	Red	1.89	5.21	1.54	4.38	**1.37**	**4.00**
	Green	1.39	1.86	1.09	1.76	**1.07**	**1.51**
	Blue	0.65	1.23	0.65	0.86	**0.58**	**0.77**
ytma49_042003	Red	15.30	5.79	3.13	**2.58**	**2.66**	2.94
	Green	5.02	8.47	1.93	**0.59**	**1.72**	0.61
	Blue	18.37	15.92	0.70	0.96	**0.55**	**0.83**
ytma49_042203	Red	**2.68**	3.24	2.78	3.17	2.80	**2.77**
	Green	**1.85**	0.77	2.08	0.73	2.24	**0.58**
	Blue	0.63	1.99	0.43	**1.84**	**0.54**	2.06
ytma49_042403	Red	2.89	3.38	**2.02**	2.67	2.22	**2.30**
	Green	1.72	1.07	**1.14**	0.96	1.16	**0.93**
	Blue	0.77	1.00	0.70	**0.83**	**0.49**	0.87
ytma49_072303	Red	1.70	3.19	1.09	1.97	**1.04**	**1.73**
	Green	1.29	1.18	0.85	0.84	**0.73**	**0.76**
	Blue	0.36	0.72	0.28	0.63	**0.20**	**0.40**
ytma49_111003	Red	3.05	3.87	2.97	4.58	**2.74**	**3.60**
	Green	2.61	1.85	**2.60**	2.23	2.61	**1.58**
	Blue	1.16	1.59	1.09	1.70	**0.77**	**1.20**
ytma49_111303	Red	1.73	5.44	1.43	3.71	**1.38**	**3.35**
	Green	1.55	2.41	**1.30**	2.03	1.31	**1.69**
	Blue	0.84	1.68	0.88	**1.17**	**0.59**	**1.17**
ytma55_030603	Red	2.69	4.32	**2.66**	4.61	2.99	**3.60**
	Green	**2.26**	1.89	2.31	1.86	2.78	**1.46**
	Blue	1.04	2.06	**0.77**	1.96	0.85	**1.63**

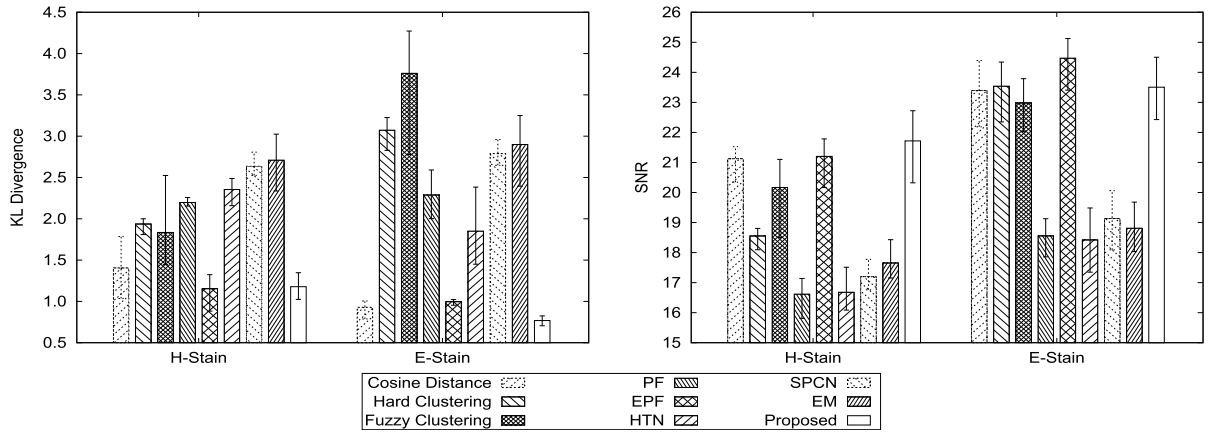

Fig. 3. Performance analysis of different clustering algorithms, dissimilarity measures, and stain separation algorithms on CMU data set using mean value of each index with error bar: A good stain separation method should produce lower value of symmetric KL divergence and higher value of SNR.

for E-stain. All the results reported in Table II confirm that the proposed algorithm performs better than the existing blind stain estimation methods.

B. Evaluation of Stain Separation

To establish the effectiveness of the proposed method in stain separation, extensive experiment is performed on CMU data set as it has stain decomposition ground-truth corresponding to each image. The associated results are reported in Fig. 3 with respect to symmetric KL divergence and SNR. Fig. 3 shows the mean value of each quantitative index along with error bar for each of the algorithms compared. The mean, maximum, and minimum values of each index are calculated for individual stain, considering three H&E stained images of CMU data set. From the results reported in Fig. 3, it is found that the proposed dissimilarity measure attains lower mean values of symmetric KL divergence and higher mean values of SNR for both the stains, with respect to cosine distance. Also, the proposed rough-fuzzy clustering algorithm provides higher mean SNR and lower values of KL divergence in all the cases, with respect to both hard and fuzzy clustering. Moreover, the difference among mean, minimum, and maximum values

TABLE II

COMPARATIVE PERFORMANCE ANALYSIS OF DIFFERENT ALGORITHMS ON UCSB DATA SET: σ_X (IN 10^{-2} SCALE) REPRESENTS THE STANDARD DEVIATION OF THE ESTIMATED STAIN VECTORS OF X-STAIN, COMPUTED OVER ALL IMAGES OF THE SAME BIOPSY SET, AND X $\in$ {H, E}

Different Biopsy Sets	Different Channels	PF		HTN		EPF		SPCN		EM		Proposed Method	
		σ_H	σ_E	σ_H	σ_E	σ_H	σ_E	σ_H	σ_E	σ_H	σ_E	σ_H	σ_E
ytma10_010704	Red	3.04	2.72	2.67	3.25	2.49	**2.10**	**2.42**	3.93	2.45	4.10	2.84	2.35
	Green	2.23	2.01	1.68	0.97	2.17	1.03	1.66	0.73	1.61	**0.69**	**1.27**	0.89
	Blue	2.67	5.79	1.14	2.43	**0.78**	2.90	1.01	2.55	0.92	2.51	1.64	**1.86**
ytma12_010804	Red	1.99	**3.79**	**1.37**	5.79	2.02	8.31	2.20	6.26	2.08	7.73	3.59	4.14
	Green	2.16	2.82	**1.07**	1.82	2.20	**1.13**	1.80	2.14	1.66	2.54	2.67	1.60
	Blue	1.72	6.81	**0.55**	1.30	0.72	1.58	0.79	1.36	0.83	1.56	0.96	**1.06**
ytma23_022103	Red	1.77	**3.43**	2.39	5.36	2.33	6.73	**1.07**	5.75	1.18	7.27	1.37	4.00
	Green	1.95	**0.46**	2.25	1.59	2.62	0.64	1.10	1.81	1.16	2.21	**1.07**	1.51
	Blue	1.31	3.34	0.70	1.57	0.92	1.50	0.86	1.71	0.89	1.86	**0.58**	**0.77**
ytma49_042003	Red	3.11	2.11	3.17	1.86	3.67	**0.55**	3.14	2.98	4.56	4.53	**2.66**	2.94
	Green	2.98	2.02	2.35	0.45	3.50	**0.45**	2.44	0.74	3.40	0.96	**1.72**	0.61
	Blue	1.09	3.67	**0.55**	0.98	1.42	1.39	0.79	1.18	1.21	1.42	**0.55**	**0.83**
ytma49_042203	Red	2.29	**2.18**	4.04	3.13	2.13	5.97	1.99	3.36	**1.93**	3.88	2.80	2.77
	Green	2.95	1.40	3.81	0.92	2.43	1.21	**2.02**	0.84	2.06	1.18	2.24	**0.58**
	Blue	1.88	3.72	1.15	2.12	0.97	2.99	0.60	2.03	0.69	**2.02**	**0.54**	2.06
ytma49_042403	Red	3.08	3.13	3.42	3.67	3.03	**0.49**	2.99	4.89	3.39	6.66	**2.22**	2.30
	Green	3.16	3.18	2.55	0.96	3.09	**0.35**	2.38	1.38	2.72	1.67	**1.16**	0.93
	Blue	1.04	5.38	0.63	**0.47**	0.79	1.09	0.93	0.64	0.92	0.80	**0.49**	0.87
ytma49_072303	Red	2.09	2.63	2.49	2.82	2.73	2.60	1.99	**1.57**	2.52	1.99	**1.04**	1.73
	Green	2.48	1.22	2.55	0.95	3.39	**0.14**	2.15	0.66	2.67	0.95	**0.73**	0.76
	Blue	0.57	1.43	0.38	0.80	0.64	0.79	0.46	0.79	0.36	0.98	**0.20**	**0.40**
ytma49_111003	Red	1.90	13.17	1.64	6.94	5.66	14.97	4.00	9.65	**1.62**	8.12	2.74	**3.60**
	Green	2.60	11.29	1.61	3.49	7.44	14.24	1.69	5.79	**1.45**	4.63	2.61	**1.58**
	Blue	3.62	10.73	1.23	2.79	4.37	12.09	9.77	4.17	1.29	2.62	**0.77**	**1.20**
ytma49_111303	Red	2.15	6.12	**1.20**	6.71	3.39	10.67	1.44	6.85	1.63	8.87	1.38	**3.35**
	Green	2.52	1.75	**1.30**	2.46	4.45	1.78	1.56	2.85	1.75	3.27	1.31	**1.69**
	Blue	1.50	4.30	**0.24**	2.34	1.37	2.49	0.34	2.31	0.55	2.70	0.59	**1.17**
ytma55_030603	Red	2.18	7.85	1.88	16.56	2.41	5.76	1.35	5.22	**1.25**	7.60	2.99	**3.60**
	Green	3.39	3.90	1.81	2.09	3.34	**1.34**	1.48	2.36	**1.37**	3.19	2.78	1.46
	Blue	2.73	8.20	0.67	8.32	**0.53**	**1.57**	0.70	1.62	0.67	2.28	0.85	1.63

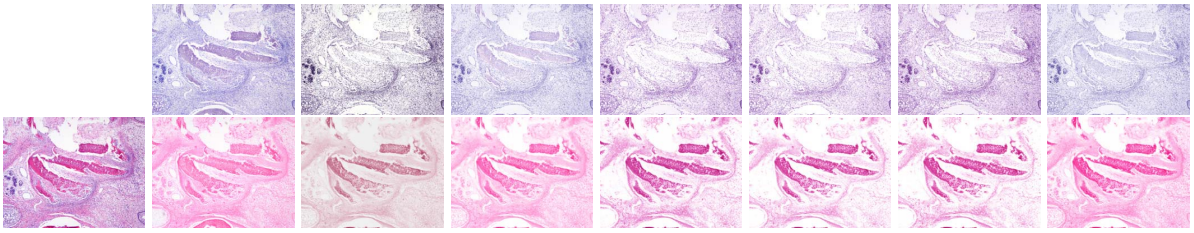

(a) CMU image (b) GT (c) PF (d) EPF (e) HTN (f) SPCN (g) EM (h) Proposed

Fig. 4. CMU image_1, ground-truth stain spectra, and estimated stain spectra obtained using different stain separation methods (top: H-stain; bottom: E-stain).

of each index for the proposed dissimilarity measure and rough-fuzzy clustering is significantly smaller as compared to that of other approaches.

The results reported in Fig. 3 also confirm that the proposed method provides lower values for KL divergence and higher values of SNR, with respect to most of the existing stain separation algorithms, while EPF performs slightly better than the proposed approach, with respect to KL divergence for H-stain and SNR for E-stain. Fig. 4 depicts an example of qualitative comparison of stain separation by different methods. From Fig. 4, it is evident that only the proposed method and EPF can extract the intrinsic structures of the biological components, highlighted by H-stain and E-stain. But, the main advantage of the proposed approach over EPF is that it is also applicable in the situation where more than two stains exist.

C. Evaluation of Color Constancy

The within-image and within-biopsy set color consistency of the proposed method as well as other color normalization methods are evaluated on UCSB data set using existing NMI and two proposed indices, namely, BiCC and WsCC. The comparative performance of different methods is analyzed using box and whisker plots, and p-values computed through both paired-t (one-tailed) and Wilcoxon signed-rank (one-tailed) tests. Fig. 5 presents the box and whisker plots of three quantitative indices, where the top and bottom boundaries of each box represent upper and lower quartiles, respectively, central line represents the median, whiskers are extended to three standard deviations from mean, and the outliers are represented by '+'. The corresponding statistical significance analysis, with respect to both Wilcoxon signed-rank and paired-t tests, is presented in Table III.

From the results reported in Fig. 5 and Table III, it is evident that the proposed circular dissimilarity measure provides higher mean and median values of NMI, BiCC, and WsCC as compared to that of cosine distance. Also, the performance of the proposed dissimilarity measure is significantly better than the cosine distance, with respect to both paired-t and

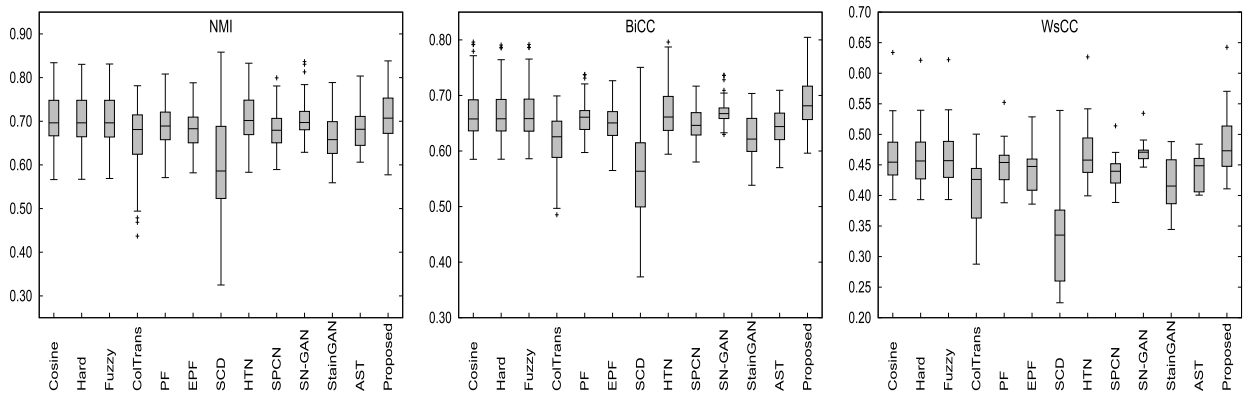

Fig. 5. Performance of different clustering algorithms, dissimilarity measures, and color normalization methods on UCSB data set using box and whisker plots for NMI, BiCC, and WsCC: A good color normalization method should produce higher values of these three indices.

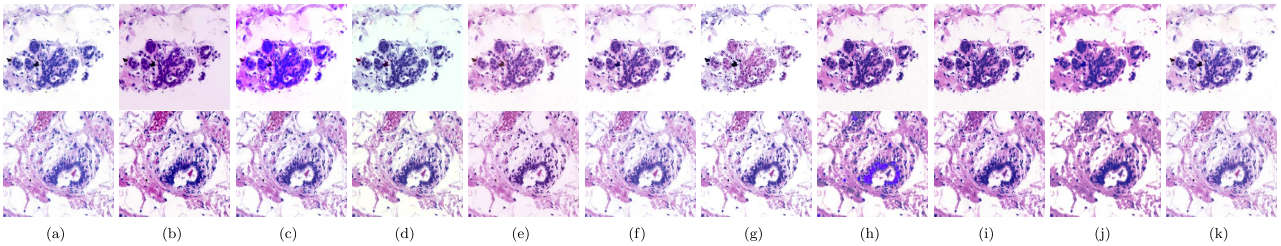

Fig. 6. (a) Original images of UCSB data set; and color normalized images obtained using different color normalization methods: (b) ColTrans, (c) PF, (d) EPF, (e) SCD, (f) HTN, (g) SPCN, (h) SN-GAN, (i) StainGAN, (j) AST, and (k) proposed.

TABLE III
STATISTICAL SIGNIFICANCE ANALYSIS OF DIFFERENT CLUSTERING ALGORITHMS, DISSIMILARITY MEASURES, AND COLOR NORMALIZATION METHODS, WITH RESPECT TO PROPOSED METHOD, ON UCSB DATA: BOTH PAIRED-*t* AND WILCOXON SIGNED-RANK TESTS ARE USED. THE P-VALUE, MARKED IN ITALICS, INDICATES THE PROPOSED METHOD IS BETTER THAN THE EXISTING ONE, BUT NOT SIGNIFICANTLY

Different Methods	NMI		BiCC		WsCC	
	Wilcoxon	Paired-*t*	Wilcoxon	Paired-*t*	Wilcoxon	Paired-*t*
Cosine Distance	2.71E-11	1.35E-13	1.75E-11	2.71E-17	2.53E-03	5.17E-06
Hard Clustering	3.27E-11	8.73E-13	1.75E-11	2.28E-19	2.53E-03	5.10E-07
Fuzzy Clustering	1.75E-11	9.00E-12	1.75E-11	2.13E-18	2.53E-03	2.30E-06
ColTrans	3.13E-06	2.45E-06	4.94E-11	1.09E-13	3.46E-03	3.81E-03
PF	3.43E-04	1.52E-04	8.73E-07	3.49E-08	*1.01E-01*	2.67E-02
EPF	1.08E-05	9.56E-07	7.76E-09	1.22E-10	1.42E-02	8.70E-03
SCD	1.43E-10	1.71E-14	1.75E-11	3.22E-22	2.53E-03	2.37E-05
HTN	4.46E-07	4.87E-06	2.16E-11	2.24E-14	2.53E-03	8.75E-05
SPCN	2.91E-06	4.66E-07	1.81E-08	1.76E-10	1.09E-02	7.95E-03
SN-GAN	*3.39E-01*	*2.30E-01*	1.02E-03	2.09E-04	*1.93E-01*	*1.51E-01*
StainGAN	1.80E-06	1.55E-07	1.01E-10	5.93E-14	3.46E-03	2.22E-03
AST	1.53E-03	6.18E-04	3.92E-09	7.46E-11	1.42E-02	9.66E-03

Wilcoxon signed-rank tests considering 95% confidence level. In order to establish the significance of rough-fuzzy clustering over its hard and fuzzy counter parts, the comparative results are also reported in Fig. 5 and Table III. From the results, it can be seen that the proposed rough-fuzzy circular clustering algorithm provides significantly higher NMI, BiCC, and WsCC values, compared to both hard and fuzzy clustering, on UCSB data set. The significantly better performance of the proposed algorithm is achieved due to the fact that the theory of rough sets can efficiently deal with uncertainty, vagueness and incompleteness in stain class definition.

Finally, the results reported in Fig. 5 and Table III ensure that the proposed method provides highest mean and median values, with respect to NMI, BiCC, and WsCC. Moreover, both Wilcoxon and paired-*t* tests show that the proposed method performs significantly better than state-of-the-art color normalization algorithms except SN-GAN [26]. The proposed method provides better performance than SN-GAN [26], but not significantly, with respect to both Wilcoxon and paired-*t* tests in case of NMI and WsCC. The qualitative performance analysis of different methods on UCSB data set is presented in Fig. 6. From the results reported in Table III and Fig. 5-6, it can be observed that the proposed method outperforms other existing methods as per the color consistency after normalization is concerned.

V. CONCLUSION

The color normalization in histological images is a fundamental task as the presence of color inconsistency among the images may degrade the performance of automated histological image analysis. In this regard, the main contributions of this paper are as follows:

- development of a new rough-fuzzy circular clustering algorithm for color normalization, which judiciously integrates the merits of rough sets and fuzzy set;
- introducing a new dissimilarity measure to deal with the circular nature of hue values;
- introducing a weighted hue histogram, integrating the information of both saturation and local neighborhood;
- defining some new quantitative indices to evaluate the color constancy among H&E stained histological images after color normalization; and
- demonstrating the efficacy of the proposed method, along with a comparison with existing algorithms, on publicly available standard H&E stained histological images.

The proposed method addresses the physical constraints such as the overlapping nature of histochemical stains as

well as the non-negativity of stain color appearance and stain density matrices. It is evident from both quantitative and qualitative results that the proposed method outperforms other existing color normalization approaches, in terms of satisfying the physical constraints and maintaining the within-image and between-image color constancy within a single biopsy set after color normalization. Moreover, the proposed algorithm does not require any prior information other than the number of stains involved in staining routine of histological images.

Acknowledgment

This publication is an outcome of the R&D work undertaken in the project under the Visvesvaraya PhD Scheme of Ministry of Electronics and Information Technology, Government of India, being implemented by Digital India Corporation.

References

[1] F. Ghaznavi, A. Evans, A. Madabhushi, and M. Feldman, "Digital imaging in pathology: Whole-slide imaging and beyond," *Annu. Rev. Pathol., Mech. Disease*, vol. 8, pp. 331–359, Jan. 2013.

[2] J. I. Epstein, W. C. Allsbrook, Jr., M. B. Amin, and L. L. Egevad, "Update on the Gleason grading system for prostate cancer: Results of an international consensus conference of urologic pathologists," *Adv. Anatomic Pathol.*, vol. 13, no. 1, pp. 57–59, 2006.

[3] A. M. Khan, N. Rajpoot, D. Treanor, and D. Magee, "A nonlinear mapping approach to stain normalization in digital histopathology images using image-specific color deconvolution," *IEEE Trans. Biomed. Eng.*, vol. 61, no. 6, pp. 1729–1738, Jun. 2014.

[4] L. Peter *et al.*, "Leveraging random forests for interactive exploration of large histological images," in *Proc. Int. Conf. Med. Image Comput. Comput.-Assist. Intervent.*, 2014, pp. 1–8.

[5] G. D. Finlayson, S. D. Hordley, and P. M. Hubel, "Color by correlation: A simple, unifying framework for color constancy," *IEEE Trans. Pattern Anal. Mach. Intell.*, vol. 23, no. 11, pp. 1209–1221, Nov. 2001.

[6] K. Nguyen, A. Sarkar, and A. K. Jain, "Structure and context in prostatic gland segmentation and classification," in *Proc. Int. Conf. Med. Image Comput. Comput.-Assist. Intervent.*, 2012, pp. 115–123.

[7] L. Gorelick *et al.*, "Prostate histopathology: Learning tissue component histograms for cancer detection and classification," *IEEE Trans. Med. Imag.*, vol. 32, no. 10, pp. 1804–1818, Oct. 2013.

[8] A. Tabesh *et al.*, "Multifeature prostate cancer diagnosis and Gleason grading of histological images," *IEEE Trans. Med. Imag.*, vol. 26, no. 10, pp. 1366–1378, Oct. 2007.

[9] S. Kothari *et al.*, "Automatic batch-invariant color segmentation of histological cancer images," in *Proc. IEEE Int. Symp. Biomed. Imag., Nano Macro*, Mar./Apr. 2011, pp. 657–660.

[10] A. Basavanhally and A. Madabhushi, "EM-based segmentation-driven color standardization of digitized histopathology," *Proc. SPIE*, vol. 8676, Mar. 2013, Art. no. 86760G.

[11] E. Reinhard, M. Adhikhmin, B. Gooch, and P. Shirley, "Color transfer between images," *IEEE Comput. Graph. Appl.*, vol. 21, no. 5, pp. 34–41, Sep./Oct. 2001.

[12] D. L. Ruderman, T. W. Cronin, and C.-C. Chiao, "Statistics of cone responses to natural images: Implications for visual coding," *J. Opt. Soc. Amer. A, Opt. Image Sci.*, vol. 15, no. 8, pp. 2036–2045, 1998.

[13] Y.-Y. Wang, S.-C. Chang, L.-W. Wu, S. T. Tsai, and Y.-N. Sun, "A color-based approach for automated segmentation in tumor tissue classification," in *Proc. 29th Annu. Int. Conf. IEEE Eng. Med. Biol. Soc.*, Aug. 2007, pp. 6576–6579.

[14] W. W. Parson, *Modern Optical Spectroscopy*, vol. 2. Berlin, Germany: Springer, 2007.

[15] A. C. Ruifrok and D. A. Johnston, "Quantification of histochemical staining by color deconvolution," *Anal. Quant. Cytol. Histol.*, vol. 23, no. 4, pp. 291–299, Aug. 2001.

[16] A. C. Ruifrok, R. L. Katz, and D. A. Johnston, "Comparison of quantification of histochemical staining by hue-saturation-intensity (HSI) transformation and color-deconvolution," *Appl. Immunohistochem. Mol. Morphol.*, vol. 11, no. 1, pp. 85–91, 2003.

[17] A. Rabinovich, S. Agarwal, C. Laris, J. H. Price, and S. J. Belongie, "Unsupervised color decomposition of histologically stained tissue samples," in *Proc. 16th Int. Conf. Neural Inf. Process. Syst.* Cambridge, MA, USA: MIT Press, 2003, pp. 667–674.

[18] J. Newberg and R. F. Murphy, "A framework for the automated analysis of subcellular patterns in human protein atlas images," *J. Proteome Res.*, vol. 7, no. 6, pp. 2300–2308, 2008.

[19] M. Macenko *et al.*, "A method for normalizing histology slides for quantitative analysis," in *Proc. IEEE Int. Symp. Biomed. Imag., Nano Macro*, Jun./Jul. 2009, pp. 1107–1110.

[20] M. Niethammer, D. Borland, J. S. Marron, J. Woosley, and N. E. Thomas, "Appearance normalization of histology slides," in *Proc. Int. Workshop Mach. Learn. Med. Imag.*, 2010, pp. 58–66.

[21] M. Gavrilovic *et al.*, "Blind color decomposition of histological images," *IEEE Trans. Med. Imag.*, vol. 32, no. 6, pp. 983–994, Jun. 2013.

[22] X. Li and K. N. Plataniotis, "A complete color normalization approach to histopathology images using color cues computed from saturation-weighted statistics," *IEEE Trans. Biomed. Eng.*, vol. 62, no. 7, pp. 1862–1873, Jul. 2015.

[23] X. Li and K. N. Plataniotis, "Blind stain decomposition for histopathology images using circular nature of chroma components," in *Proc. IEEE Int. Conf. Acoust., Speech Signal Process. (ICASSP)*, Apr. 2015, pp. 877–881.

[24] Y.-K. Lai and P. L. Rosin, "Efficient circular thresholding," *IEEE Trans. Image Process.*, vol. 23, no. 3, pp. 992–1001, Mar. 2014.

[25] A. Vahadane *et al.*, "Structure-preserving color normalization and sparse stain separation for histological images," *IEEE Trans. Med. Imag.*, vol. 35, no. 8, pp. 1962–1971, Aug. 2016.

[26] F. G. Zanjani, S. Zinger, B. E. Bejnordi, J. A. W. M. van der Laak, and P. H. N. D. With, "Stain normalization of histopathology images using generative adversarial networks," in *Proc. 15th Int. Symp. Biomed. Imag. (ISBI)*, Apr. 2018, pp. 573–577.

[27] A. Bentaieb and G. Hamarneh, "Adversarial stain transfer for histopathology image analysis," *IEEE Trans. Med. Imag.*, vol. 37, no. 3, pp. 792–802, Mar. 2018.

[28] T. Wollmann, C. S. Eijkman, and K. Rohr, "Adversarial domain adaptation to improve automatic breast cancer grading in lymph nodes," in *Proc. IEEE 15th Int. Symp. Biomed. Imag. (ISBI)*, Apr. 2018, pp. 582–585.

[29] M. T. Shaban, C. Baur, N. Navab, and S. Albarqouni, "Staingan: Stain style transfer for digital histological images," in *Proc. IEEE 16th Int. Symp. Biomed. Imag. (ISBI)*, Apr. 2019, pp. 953–956.

[30] X. Li and K. N. Plataniotis, "Circular mixture modeling of color distribution for blind stain separation in pathology images," *IEEE J. Biomed. Health Inform.*, vol. 21, no. 1, pp. 150–161, Jan. 2017.

[31] Z. Pawlak, *Rough Sets: Theoretical Aspects of Reasoning About Data*. Dordrecht, The Netherlands: Kluwer, 1991.

[32] L. A. Zadeh, "Fuzzy sets," *Inf. Control*, vol. 8, no. 3, pp. 338–353, Jun. 1965.

[33] P. Maji and S. Mahapatra, "Rough-fuzzy circular clustering for color normalization of histological images," *Fundam. Inform.*, vol. 164, no. 1, pp. 103–117, 2019.

[34] A. Hanbury, "Circular statistics applied to colour images," in *Proc. 8th Comput. Vis. Winter Workshop*, 2003, vol. 91, nos. 1–2, pp. 53–71.

[35] L. Szilagyi, Z. Benyo, S. M. Szilagyi, and H. S. Adam, "MR brain image segmentation using an enhanced fuzzy C-means algorithm," in *Proc. 25th Annu. Int. Conf. IEEE Eng. Med. Biol. Soc.*, Sep. 2003, pp. 724–726.

[36] N. I. Fisher, *Statistical Analysis of Circular Data*. Cambridge, U.K.: Cambridge Univ. Press, 1995.

[37] G. James, *Modern Engineering Mathematics* . London, U.K.: Pearson, 2015.

[38] L. G. Nyul, J. K. Udupa, and X. Zhang, "New variants of a method of MRI scale standardization," *IEEE Trans. Med. Imag.*, vol. 19, no. 2, pp. 143–150, Feb. 2000.

[39] M. T. McCann, J. Majumdar, C. Peng, C. A. Castro, and J. Kovačević, "Algorithm and benchmark dataset for stain separation in histology images," in *Proc. IEEE Int. Conf. Image Process. (ICIP)*, Oct. 2014, pp. 3953–3957.

[40] P. J. Rousseeuw, "Silhouettes: A graphical aid to the interpretation and validation of cluster analysis," *J. Comput. Appl. Math.*, vol. 20, no. 1, pp. 53–65, 1987.

[41] E. D. Gelasca, J. Byun, B. Obara, and B. S. Manjunath, "Evaluation and benchmark for biological image segmentation," in *Proc. IEEE Int. Conf. Image Process.*, Oct. 2008, pp. 1816–1819.

[42] K. Plataniotis and A. N. Venetsanopoulos, *Color Image Processing and Applications*. New York, NY, USA: Springer-Verlag, 2000.